Climate Dynamics
https://doi.org/10.1007/s00382-018-4164-9

Future climate change enhances rainfall seasonality in a regional model of western Maritime Continent

Suchul Kang[1] · **Eun-Soon Im**[2] · **Elfatih A. B. Eltahir**[3]

Received: 28 July 2017 / Accepted: 28 February 2018

Abstract
In this study, future changes in rainfall due to global climate change are investigated over the western Maritime Continent based on dynamically downscaled climate projections using the MIT Regional Climate Model (MRCM) with 12 km horizontal resolution. A total of nine 30-year regional climate projections driven by multi-GCMs projections (CCSM4, MPI-ESM-MR and ACCESS1.0) under multi-scenarios of greenhouse gases emissions (Historical: 1976–2005, RCP4.5 and RCP8.5: 2071–2100) from phase 5 of the Coupled Model Inter-comparison Project (CMIP5) are analyzed. Focusing on dynamically downscaled rainfall fields, the associated systematic biases originating from GCM and MRCM are removed based on observations using Parametric Quantile Mapping method in order to enhance the reliability of future projections. The MRCM simulations with bias correction capture the spatial patterns of seasonal rainfall as well as the frequency distribution of daily rainfall. Based on projected rainfall changes under both RCP4.5 and RCP8.5 scenarios, the ensemble of MRCM simulations project a significant decrease in rainfall over the western Maritime Continent during the inter-monsoon periods while the change in rainfall is not relevant during wet season. The main mechanism behind the simulated decrease in rainfall is rooted in asymmetries of the projected changes in seasonal dynamics of the meridional circulation along different latitudes. The sinking motion, which is marginally positioned in the reference simulation, is enhanced and expanded under global climate change, particularly in RCP8.5 scenario during boreal fall season. The projected enhancement of rainfall seasonality over the western Maritime Continent suggests increased risk of water stress for natural ecosystems as well as man-made water resources reservoirs.

1 Introduction

Rainfall over the Maritime Continent reflects a set of complex non-linear processes, which are acting on different spatial and temporal scales. On the large-scale and low-frequency modes, the Maritime Continent is significantly influenced by the inter-annual variability associated with Indian Ocean Dipole (IOD) and El-Nino Southern Oscillation (ENSO) (Ashok et al. 2001; Wang et al. 2003; Chang et al. 2004; Juneng and Tangang 2005; Tangang et al. 2012; Salimun et al. 2014, 2015), the Hadley and Walker circulations (Neale and Slingo 2003), and the Asian–Australian monsoon system through teleconnections (Chang et al. 2005; Moron et al. 2009; Robertson et al. 2011; Juneng and Tangang 2010; Tangang et al. 2012). On the other hand, the convective activities at the local and regional scales generated by the orography and sea-breeze convergence also play a critical role in shaping the mean climate over the Maritime Continent through the modulation of the diurnal variation of rainfall (Neale and Slingo 2003; Qian 2008; Im and Eltahir 2017).

The limited accuracy of climate models, their inability to resolve multi-scale phenomena and their interactions, and the insufficient level of our current understanding of the associated physical processes result in a high level of uncertainty regarding future changes in rainfall over the Maritime Continent. The Working Group I for the Fifth Assessment Report (AR5) of the Intergovernmental

✉ Eun-Soon Im
ceim@ust.hk

[1] Singapore-MIT Alliance for Research and Technology (SMART), Center for Environmental Sensing and Modeling (CENSAM), Singapore, Singapore

[2] Division of Environment and Sustainability, Department of Civil and Environmental Engineering, Academic Building 3594, The Hong Kong University of Science and Technology, Clear Water Bay, Kowloon, Hong Kong, China

[3] Ralph M. Parsons Laboratory, Massachusetts Institute of Technology, Cambridge, MA 02139, USA

Published online: 10 March 2018

Panel on Climate Change (IPCC) (Christensen et al. 2013) assessed future changes in rainfall on the basis of global climate models (GCMs) projections under Representative Concentration Pathways (RCPs) emission scenarios, participating in Coupled Model Intercomparison Project Phase 5 (CMIP5, Taylor et al. 2012). For the western Maritime Continent (defined here as 10°S–8°N, and 95°E–120°E), the projected changes in rainfall exhibit a mixed signal with both increasing and decreasing patterns. More importantly, most of regions around the western Maritime Continent suffer from the lack of inter-model agreement: there are little robust patterns of future rainfall projections in either change sign (e.g. increase or decrease) or magnitude (e.g. strong or weak) under global climate change.

GCMs reveal significant deficiency in simulating key climate features over the Maritime Continent. More precise representation of land-sea distribution and complex topography can improve climate simulations over the Maritime Continent (e.g. Arakawa and Kitoh 2005; Schiemann et al. 2014). Large-scale circulations and variability (e.g. ENSO) play an important role in shaping the main pattern and variability in the climate of the Maritime Continent. However, GCMs seem to perform poorly in simulating the climate of this region. Previous studies have showed that GCMs are not accurate enough in simulating the detailed characteristics of rainfall over the Maritime Continent (Zhou and Wang 2006; Qian 2008; Ploshay and Lau 2010; Love et al. 2011) mainly due to their coarse resolution. The typical horizontal resolution of more than 100 km is not suitable to resolve the distinct geography of the region, which features several land masses with steep topography (e.g. Malay Peninsula, Sumatra, Borneo and Java islands), surrounded by warm and shallow ocean water. In particular, GCMs reveal their deficiencies in the simulation of convective processes varying diurnally and regionally, which in turn induce substantial errors in the propagation of the diurnal phase and amplitude of the rainfall that are critical for determining the mean climate over the Maritime continent.

Regional climate models (RCMs) are useful tools for improving the simulation of rainfall climatology in terms of daily or sub-daily characteristics at the local and regional scales. A significant body of research has demonstrated the positive impact of higher resolution on rainfall simulations such as diurnal variation and extremes based on the climate modeling studies (Liang et al. 2004; Ploshay and Lau 2010; Love et al. 2011; Peatman et al. 2015; Im and Eltahir 2017). In particular, Im and Eltahir (2017) stress that a realistic coastline and a sharp gradient of elevation, as captured by a high resolution grid system, would enhance the local circulation associated with land-sea breeze and topographic complexity, and hence bring more physical realism to representation of rainfall formation within models.

In this study, we project future changes in rainfall under global climate change over the western Maritime Continent using the latest version of the Massachusetts Institute of Technology (MIT) regional climate model (MRCM) that has been tested by previous studies in its ability to simulate rainfall characteristics including time-mean fields as well as diurnal variation over this region (Im and Eltahir 2017). Significant efforts to produce high resolution climate projections have been recently made based on the dynamical downscaling using RCMs within the well-coordinated framework (e.g. Coordinated Regional Climate Downscaling Experiment, CORDEX; Giorgi et al. 2012). However, this research effort mostly targeted North America, Africa, Europe and East Asia (Giorgi et al. 2012; Vautard et al. 2013; Lucas-Picher et al. 2013; Mariotti et al. 2014; Park et al. 2016), but not the Maritime Continent. There are a few studies that attempted to generate the dynamically-downscaled future climate information over some regions included in the Maritime Continent based on the IPCC Fourth Assessment Report (AR4) framework [e.g. global projections participating in the CMIP3 project and the Special Report on Emissions Scenarios (SRES) emission scenarios]. For instance, Loh et al. (2016) projected the weakening of the monsoon trough during the boreal winter and spring seasons, which results in drier and warmer climate over northern Borneo and Malaysia Peninsula under both high and low level emission scenarios (e.g. SRES A2 and B2). On contrary, Chotamonsak et al. (2011) showed that northern Borneo and Singapore will experience substantial increase of rainfall in winter under the middle level of emission scenario (e.g. SRES A1B). This contrast in past research results suggests great uncertainty still exists, inviting further systematic investigations. In addition, it is necessary to update our experimental protocols to reflect the latest progress (e.g. CMIP5 global projection and RCP emission scenarios).

Here, we perform the dynamical downscaling of CMIP5 projections forced by RCP4.5 and RCP8.5 emission scenarios using MRCM. For ensemble regional projections, we generate three MRCM projections driven by three different GCMs that are carefully selected through a rigorous evaluation of their reference simulations (see Sect. 2.3). Also, the mean biases of MRCM simulations are statistically corrected at the daily time-scale using the Parametric Quantile Mapping method (see Sect. 2.4). To the best of our knowledge, there is minimal literature on ensemble regional projections targeted at the western Maritime Continent, taking multi-GCMs and multi-scenarios into consideration within the IPCC AR5 framework. Therefore, the updated assessment presented in this study can provide an opportunity not only to fill the gap of climate change research over this region but also to build on previous findings and progress achieved by other research groups.

2 Model description and experimental design

2.1 The MIT regional climate model

MRCM (Im et al. 2014) used for the dynamical downscaling in this study is based on ICTP-Regional Climate Model Version 3 (RegCM3, Pal et al. 2007) but with several improvements, including coupling to the Integrated Biosphere Simulator (IBIS) land surface scheme (Winter et al. 2009), new surface albedo assignment (Marcella and Eltahir 2012), modified boundary layer height and boundary layer cloud scheme (Gianotti 2012), irrigation scheme (Marcella and Eltahir 2014), new convective cloud scheme (Gianotti and Eltahir 2014a) and new convective rainfall autoconversion scheme (Gianotti and Eltahir 2014b). As a result of such efforts that incorporate new physical schemes or modify original schemes, MRCM showed comparable or better performance in simulating key climate features across various regions (e.g., North America, West Africa, Southwest Asia, Maritime Continent) compared to other regional climate models (Winter et al. 2009; Im et al. 2014; Marcella and Eltahir 2012; Gianotti and Eltahir 2014a, b; Im and Eltahir 2017). Furthermore, Im and Eltahir (2017) demonstrate that enhanced horizontal resolution can contribute to a better capability of MRCM by comparing the results from different resolutions (27 vs. 12 km) that are performed under the same model configuration except for the horizontal resolution. On the basis of the improved performance of MRCM with 12 km horizontal resolution over the western Maritime Continent, we adopt the same version of MRCM used in Im and Eltahir (2017).

2.2 Experimental design

The MRCM domain covers the western Maritime Continent with 240 × 172 grids, centered at 0.8°S, 107°E. The horizontal resolution is 12 km which is fine enough to represent geographical complexity (Fig. 1). For detailed characterization of rainfall across geographically diverse regions, the land area within our domain is divided into nine sub-region.

In particular, Peninsula Malaysia is divided into two sub-region (west and east) while Borneo Island is divided into three sub-region (northwest, northeast, and south), based on previous studies that have emphasized distinct local rainfall patterns over the Maritime Continent (Aldrian and Susanto 2003; Tangang et al. 2008; Chen et al. 2013a; Loh et al. 2016; Juneng et al. 2016; Cruz et al. 2017). The longitude and latitude ranges for each sub-region are as follows; A: 114.3°E–119.3°E, 1.2°N–7.5°N (Borneo-Northeast), B: 108.5°E–114.3°E, 1.2°N–7.5°N (Borneo-Northwest), C: 108.5°E–119.3°E, 4.5°S–1.2°N (Borneo-South), D: 102°E–104.5°E, 1°N–5.7°N (Peninsula Malaysia-East), E: 100°E–102°E, 1°N–5.7°N (Peninsula Malaysia-West), F: 103.6°E–104.1°E, 1.18°N–1.48°N (Singapore), G: 95°E–104.5°E, 0°N–6°N (Sumatra-North), H: 95°E–106.3°E, 6°S–0°S (Sumatra-South), and I: 105°E–115.9°E, 9°S–5.7°S (Java).

For the initial and boundary conditions that are prescribed for MRCM, the output representing atmospheric conditions every 6-h simulated by three selected GCMs are downloaded from the CMIP5 data archives. CMIP5 global projections are generated by fully coupled Atmosphere–Ocean GCMs.

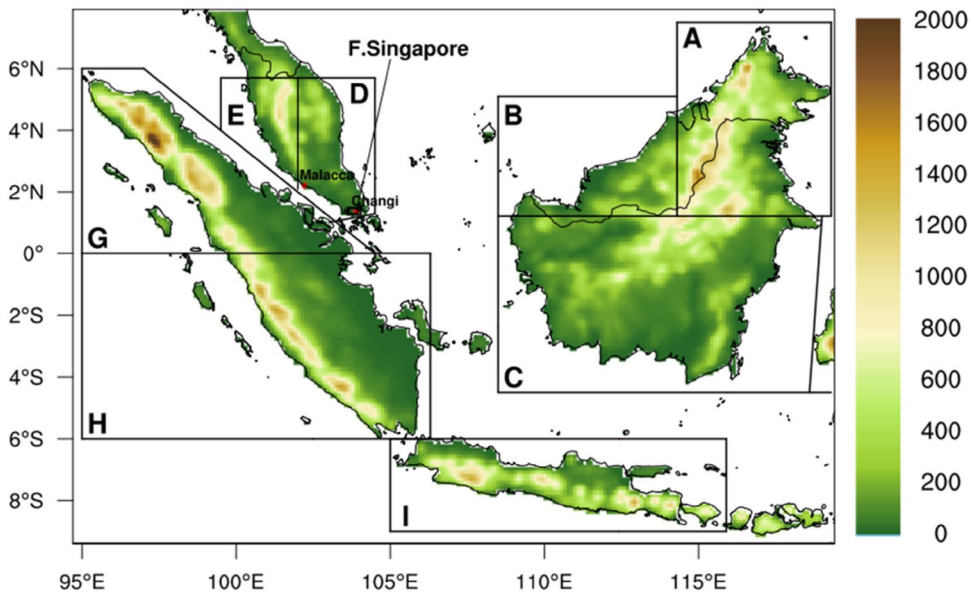

Fig. 1 MRCM simulation domain and topography (unit: m). Boxes indicate the nine sub-region used for regional analysis in this study. Two red dots indicate the in-situ observational stations at Changi (1.35°N, 103.99°E) and Malacca (2.26°N, 102.25°E) located in Singapore and Peninsula Malaysia, respectively

The reference simulation corresponds to a "historical" run in CMIP5 label, not "historicalNat" and "historicalGHG" which represent the historical simulation but with natural forcing only and historical simulation but with greenhouse gas (GHG) forcing only, respectively (Taylor et al. 2012). Therefore, the CMIP5 global projections include not only the responses to anthropogenic forcings but also natural forcings. While the reference simulation (1975–2005) is forced by historical GHGs concentration, two future projections (2070–2100) are forced by the Representative Concentration Pathway (RCP)4.5 and RCP8.5, corresponding to a medium-mitigation and business-as-usual emission scenarios (Moss et al. 2010). Therefore, a total of nine GCM projections are dynamically downscaled using the MRCM. The first year of MRCM simulations in both the reference and future periods has been discarded in the analysis as a spin-up period. The methodology for the selection of three GCMs is described in detail in Sect. 2.3.

2.3 GCMs selection

The suitable GCMs that are used to drive MRCM are selected among the CMIP5 participant models through the following steps.

1. We first select 19 models out of 28 CMIP5 GCMs which are able to capture the significant climate features over the region of Southeast Asia including the Maritime Continent based on the analysis of McSweeney et al. (2015a). Their study systematically evaluates GCMs that participated in CMIP5, and provides overall performance metrics over the continental-scale regions such as Southeast Asia, Europe and Africa.
2. We exclude the GCMs with relatively coarser horizontal resolution, such as atmospheric and oceanic component models coarser than 2° and 1.2° resolution, respectively. Through this criteria, we select six GCMs from the first 19 selected GCMs.
3. The reference simulations from the selected six GCMs are evaluated over the western Maritime Continent focusing on the relevant features of specific interest in this study. More specifically, the performances of how reasonably the models simulate rainfall, temperature, wet-bulb temperature, and humidity are assessed in terms of spatial pattern, normalized root mean square error (NRMSE) and annual cycle over land and ocean, by comparing them with Climatic Research Unit (CRU: Harris et al. 2014) and ERA Interim Reanalysis (ERA-Interim: Dee et al. 2011) data.

As a result of the screening process described above, three GCMs are finally selected: Community Climate System Model Version 4 (CCSM4), Australian Community Climate and Earth System Simulator Version 1.0 (ACCESS1.0) and Max-Planck-Institution Earth System Model running on Medium Resolution grid (MPI-ESM-MR). More information about these GCMs is presented in Table 1.

2.4 Statistical bias correction

The results simulated by any regional climate model may contain a systematic bias arising from lateral boundary conditions (i.e., global climate model) as well as imperfect RCM physics (Liang et al. 2008; Ehret et al. 2012). To enhance the reliability of future climate projections, a statistical bias correction method is applied involving the assumption that the bias in the reference simulation remains the same in the future projections. In case of the rainfall, a Parametric Quantile Mapping (PQM) is commonly used and it can effectively remove the systematic bias based on the assumption that both observed and simulated rainfall intensity distributions are well approximated by the gamma distribution (Piani et al. 2010). Here, we apply the PQM for bias correction of simulated daily rainfall. In doing this, the cumulative frequency distributions for the modeled and observed daily rainfall are calculated for each month from January to December, and simulated distribution is then fitted to observed one by matching the cumulative quantiles. As for the observational data, we use the Tropical Rainfall Measuring Mission (TRMM) 3B42 Version 7 (Huffman and Bolvin 2012) products. Since TRMM data is not available during the same period of reference simulations, 18-year (1998–2015) climatological features are compared with both GCM and MRCM simulations based on 30-year (1976–2005) climatology. To facilitate the direct comparison with MRCM results, TRMM data with $0.25° \times 0.25°$ spatial resolution is aggregated into the MRCM grid (12 km).

2.5 Estimation of rainfall seasonality

To quantitatively estimate the changes in seasonal variation of rainfall, we use a simple index (**S**) that describes the

Table 1 Descriptions of global climate models selected as lateral boundary forcings for MRCM simulation in the study

Model name	ATM resolution (lat × lon)	OCN resolution (lat × lon)	Main references
CCSM4	0.9° × 1.25°	1.11° × 0.27°–0.54°	Gent et al. (2011)
MPI-ESM-MR	T63 (~ 1.875°)	0.4° × 0.4°	Giorgetta et al. (2013)
ACCESS 1.0	1.25° × 1.875°	1/3°–1°	Bi et al. (2013)

rainfall seasonality as follows. **S** is the rainfall difference between the months with maximum and minimum monthly rainfall normalized by average monthly rainfall. **S** is helpful in assessing the seasonality in rainfall amounts between dry and wet seasons, presented in dimensionless form.

$$\mathbf{S} = \left(R_{max} - R_{min}\right) / R_{mean},$$

where, R_{mean} is average monthly rainfall, and R_{max} and R_{min} are the maximum and minimum monthly rainfall during the year, respectively.

3 Results

3.1 Verification of MRCM simulation with bias correction

The evaluation of the MRCM performance is an essential prerequisite to ensure the reliability of future projections. Prior to downscaling of "non-perfect" GCM boundary conditions, Im and Eltahir (2017) performed the dynamical downscaling of the ERA Interim reanalysis data using MRCM, so-called "perfect boundary condition" experiment, and demonstrated a reasonable performance of MRCM in simulating the spatial and temporal structure of rainfall for present-day conditions, based on the analysis of 30-year (1982–2011) climatological statistics. We then perform climate change experiments using the same version of MRCM, but driven with three different GCMs. Prior to the analysis of future changes, we examine (1) whether dynamically downscaled MRCM results provide the added value over driving GCM, and (2) whether PQM applied for the bias correction step improves the results by effectively removing the systematic bias.

Figure 2 presents the spatial distributions of climatological rainfall averaged over wet (November–December–January: NDJ) and dry (May–June–July: MJJ) seasons as well as inter-monsoon (February–March–April: FMA, August–September–October: ASO) seasons. These months are chosen based on the annual cycle of rainfall around the center of the region, near Singapore. For example, NDJ typically receives the largest seasonal and daily totals of rainfall in Singapore and neighboring islands of Indonesia and Borneo (McSweeney et al. 2015b). Model results are displayed as the ensemble mean based on the arithmetic average of three different members. MRCM ensemble mean with and without bias correction are denoted as MRCM_BC and MRCM hereafter. First of all, the added value of MRCM over GCM can be found in the pattern of seasonal variation. Since GCM overestimates rainfall during dry season (MJJ) but underestimates it during the wet season (NDJ), its seasonal variation is much smaller than that of TRMM. On the other hand, MRCM captures the seasonal variation with similar relative magnitudes to TRMM in spite of underestimation of the rainfall for both seasons. This behavior is quantitatively described by the area-averaged rainfall over land as indicated by Fig. 2. In addition to the improved seasonal variation, the spatial details captured by higher resolution can contribute to the enhancement of the added value of downscaled MRCM results. In Malay Peninsula, the area emerging with stronger rainfall in ASO and reaching the peak in NDJ is only captured in MRCM, not GCM ENS. However, MRCM produces excessive rainfall along the high mountainous region, which does not appear in TRMM observed pattern. This problematic feature of MRCM can be interpreted as the typical error simulated by other high resolution RCMs (Solman et al. 2008; Gianotti 2012). Alternatively, this discrepancy between MRCM and TRMM can partly be due to observational under-sampling where short-lived intensive rainfall could have been missed by the 3-hourly sampling period of 3B42 TRMM observation (Teo et al. 2011). Once PQM is applied to MRCM, the deficiency of MRCM raw data can be statistically corrected, suggesting the effectiveness and usefulness of PQM in correcting the systematic bias in rainfall simulations. By comparison with MRCM, MRCM_BC is in better agreement with TRMM in terms of the spatial distribution and area-averaged rainfall over land, which is to be expected.

Figure 3 shows the annual cycle of area-averaged rainfall over whole land domain. Both GCM and MRCM fail to capture a bimodal distribution with two asymmetric peaks characterized by the observed pattern in TRMM. Furthermore, GCM shows much smaller seasonality than that of TRMM because GCM overestimates rainfall from May to September but underestimates it from October to April. The improvement of MRCM is found in the seasonality, bringing it closer to TRMM. MRCM_BC tends to enhance the maximum rainfall amount, but to be less effective in correcting qualitative aspects (e.g. bimodal structure). In contrast this limited accuracy in terms of the gross pattern averaged over whole land area, MRCM_BC demonstrates encouraging performance in simulating the annual cycle and peak timing of rainfall averaged over nine sub-region (see the explanation in Fig. 5).

In order to examine the daily statistics of rainfall at local scale, we compare the frequency distribution of daily rainfall at Changi (located in Singapore) and Malacca (located in Peninsula Malaysia) stations (Fig. 4). For this analysis, in-situ observations at the Changi (1.35°N, 103.99°E) and Malacca (2.26°N, 102.25°E) stations are obtained from the Integrated Surface Database (Smith et al. 2011). To avoid large number of missing values included in Malacca station data, the analysis period is limited to the recent 15-year (2001–2015) in terms of the station and TRMM data. To facilitate the comparison, MRCM data is exacted for the last 15-year of reference simulation (1991–2005) at the grid

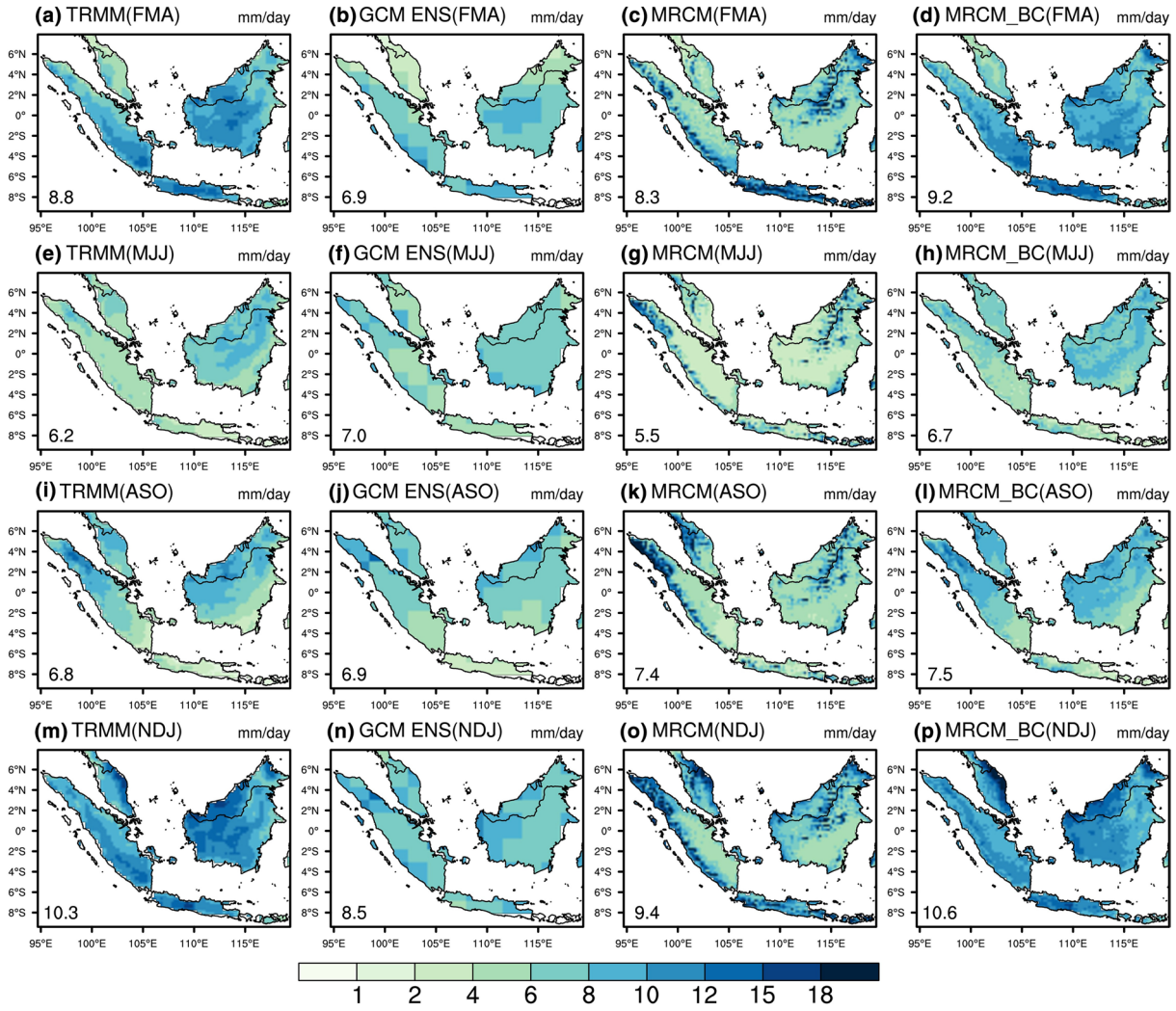

Fig. 2 Spatial distribution of seasonal rainfall for inter-monsoon seasons (FMA: **a**–**d**, ASO: **i**–**l**), and dry (MJJ: **e**–**h**), and wet (NDJ: **m**–**p**) seasons derived from the (**a, e, i, m**) TRMM, (**b, f, j, n**) ensemble mean of GCMs (denoted by GCM ENS), (**c, g, k, o**) ensemble mean of MRCMs (denoted by MRCM), and (**d, h, l, p**) ensemble mean of bias-corrected MRCMs (denoted by MRCM_BC). Area-averaged value over land is included in the bottom left corner of each plot (unit: mm/day)

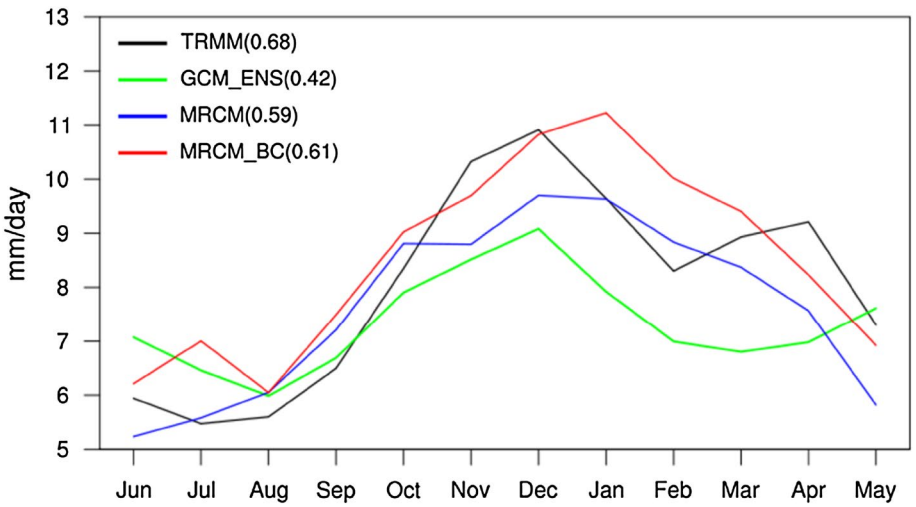

Fig. 3 Annual cycle of total rainfall (unit: mm/day) averaged over the land area of domain derived from TRMM (black), GCM_ENS (green), MRCM (blue) and MRCM_BC (red). Number in bracket indicates seasonality of rainfall

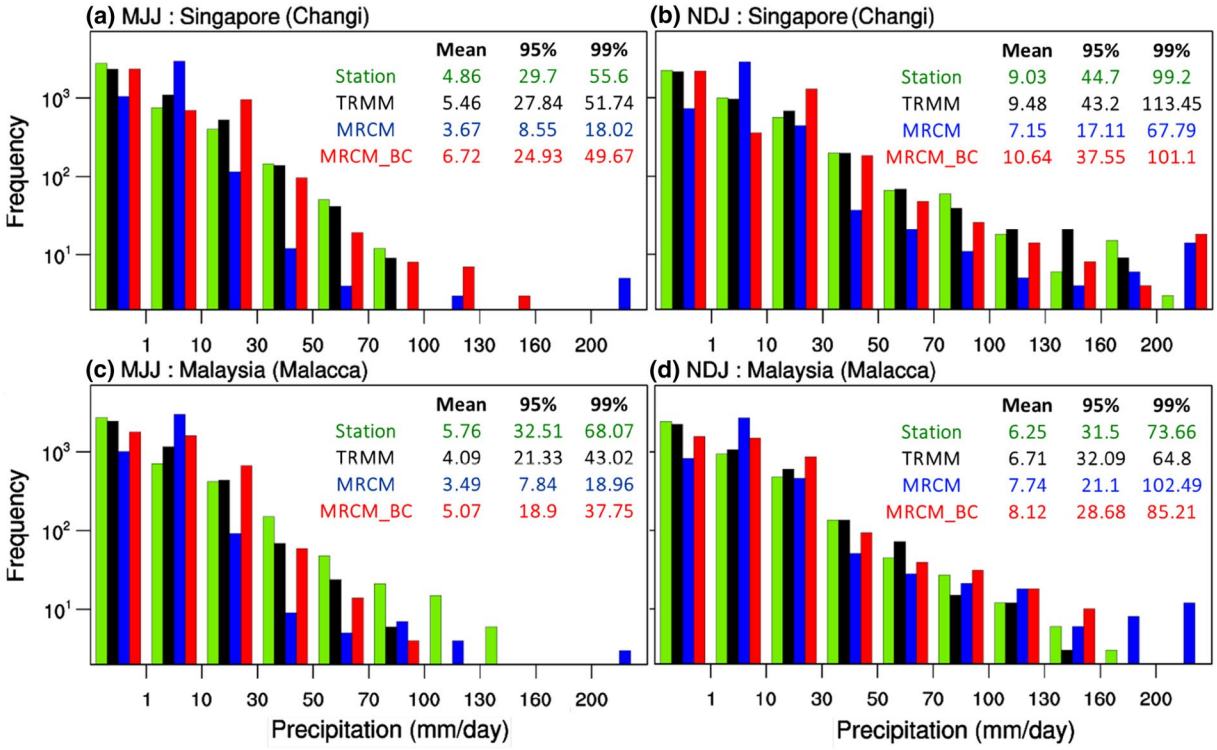

Fig. 4 Histogram of daily rainfall at Changi and Malacca stations derived from in-situ observations (green), TRMM 3B42 (black), MRCMs (blue) and MRCM_BC (red) during dry (MJJ: **a, c**) and wet (NDJ: **b, d**) seasons

points closest to the stations. For both stations, the shape of distribution is noticeably different between wet (e.g. NDJ) and dry (e.g. MJJ) seasons. The frequency of daily rainfall in wet season decreases more slowly as the intensity increases with a long tail. In general, MRCM is capable of reproducing the frequency distribution characteristics, corresponding to the wet and dry seasons. However, its accuracy is limited when looking into quantitative aspect. MRCM tends to underestimate rainfall in the range of the low to mid-intensities, but produces unrealistically extreme rainfall such as 200 mm/day that is absent in TRMM observation. The PQM application brings positive effects, reducing the errors that appeared in MRCM distribution. MRCM_BC shows a substantial improvement not only in mean value but also 95 and 99% level. However, MRCM_BC still retain significant errors in very extreme cases such as over 100 mm/day for dry season and over 200 mm/day for wet season at Changi station. By comparing the characteristics of distribution at both stations, daily rainfall at Changi station shows the larger seasonality than that at Malacca with higher mean and extremes values (e.g. 95 and 99%). MRCM_BC exhibits a skill in simulating these qualitative aspects, in spite of some quantitative discrepancies.

In summary, MRCM_BC shows reasonable performance in capturing seasonally varying patterns with respect to their spatial distributions, and also in capturing daily statistics. In the next section, we focus on the future projections of rainfall under the RCP4.5 and RCP8.5 scenarios.

3.2 Future changes in rainfall and related circulation patterns

In this section, we investigate the future rainfall projections derived from the ensemble mean of MRCM simulations forced by three GCM projections. The same bias-correction factors derived from the reference simulation are applied to the RCP future projections, under the assumption of "stationarity" implying that systematic bias does not change with time. Future changes are calculated by the difference between reference simulation (1976–2005, referred to REF) and two future projections (2071–2100) under the RCP4.5 and RCP8.5 emission scenarios (referred to RCP4.5 and RCP8.5).

Figure 5 presents the annual cycle of area-averaged rainfall across all nine sub-region depicted in Fig. 1. To investigate the MRCM_BC performance of how it reasonably captures the region-specific characteristics, the degree of accuracy in simulating peak timing and seasonality across different regions is evaluated against TRMM climatology. In general, REF is able to capture the distinct features of the annual cycle of rainfall varying from region to region due to unique geographical properties (Aldrian and Susanto

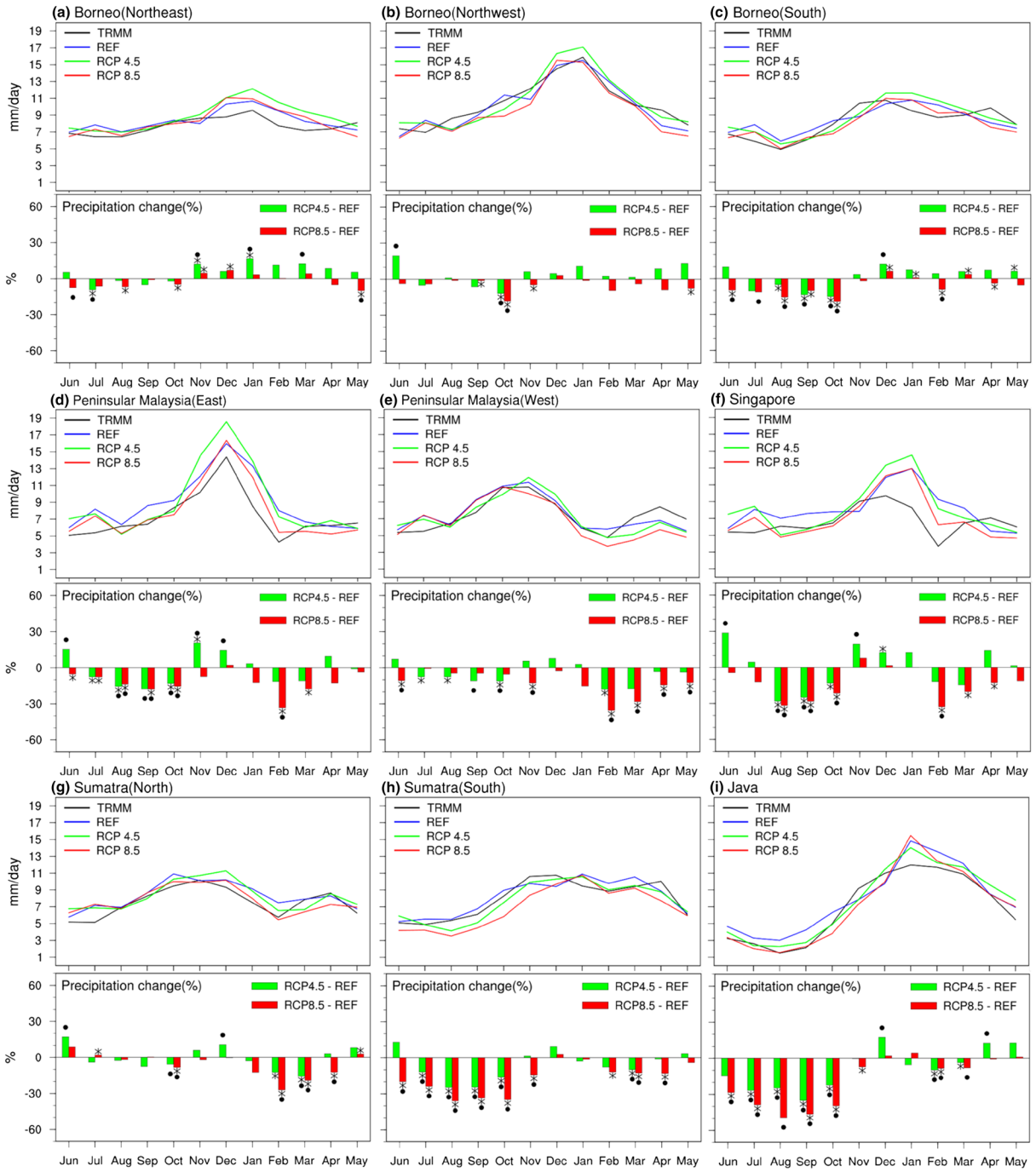

Fig. 5 Annual cycle of total rainfall (unit: mm/day) averaged over nine sub-region derived from TRMM (black), REF (blue), RCP4.5 (green) and RCP8.5 (red) and monthly rainfall change (unit: %) under RCP4.5 and RCP8.5. Asterisk indicates that three MRCMs agree in the sign of change signal. Black dot indicates that rainfall change is statistically significant at the 95% confidence level based on a two-tailed Student's t-test

2003). For example, Peninsular Malaysia is characterized by substantial difference in rainfall pattern between western and eastern parts (Tangang et al. 2008, 2017; Chen et al. 2013a, b; Loh et al. 2016; Jamaluddin et al. 2017). Loh et al. (2016) demonstrated that it is difficult for climate models to accurately reproduce the peak timing in the annual cycle of rainfall over east coast of Peninsular Malaysia. REF, simulated using high-resolution and well-optimized MRCM, apparently differentiates region-specific patterns between western and eastern parts of Peninsular Malaysia, in particular capturing the exact timing of maximum rainfall (e.g. December) over east coast. More importantly, comparing

rainfall averaged over east coast of Peninsular Malaysia and northern Borneo (both northeast and northwest) further supports the reasonable performance of MRCM_BC. REF is in a good agreement with TRMM, reproducing the different timing characterizing the maximum rainfall over these regions, being delayed by 1 month in northern Borneo compared to east coast of Peninsular Malaysia. These results are in line with the results presented in Chen et al. (2013a) that emphasized the different mechanisms of rainfall formation based on the comprehensive analysis of various observational dataset. While relatively earlier peak of rainfall in east coast of Peninsular Malaysia is mainly due to the cold surges vortex and heavy rainfall propagating from the Philippine area and Borneo, the major course of the rainfall maximum in northern Borneo is rain-producing disturbance from South China Sea (Tangang et al. 2008, 2017; Chen et al. 2013a, b). A detailed investigation of rainfall formation mechanisms across different regions is beyond the scope of this study, but the fact that REF is able to capture these regional-dependent features implicitly supports the sound physical basis of MRCM and the added value of dynamical downscaling using the high-resolution RCM. REF also shows a skill in capturing the different characteristics of annual cycle of rainfall between northwest and northeast Borneo, similar to TRMM. Rainfall pattern averaged over northwest Borneo shows the strong seasonal variation with the peak value reaching up to 15 mm/day, whereas there is weak seasonality in northeast Borneo. For other regions, the maximum rainfall peak appears to be later in Southern Sumatra and Java located at the south of equator, compared to Singapore near equator.

Moving to future rainfall changes, the differences (%, color bars in lower panel) between REF and RCP4.5 or RCP8.5 are also presented in Fig. 5 to quantitatively describe the change in rainfall under climate change conditions with respect to REF. A two-tailed Student's t test is performed for the statistical significance of future changes against REF (2071–2100 relative to 1976–2005). Black dots above color bars in Fig. 5 indicate that rainfall changes are statistically significant at the 95% level. In addition to the typical statistical significance test, the consistency among the different ensemble members is also assessed. The asterisk above bar indicates that the rainfall changes from the three MRCM members all have the same sign of increase or decrease, and hence future change seems to be robust behavior in response to rising concentrations of CO_2 independent of the selected GCM boundary forcing.

For future rainfall changes, the most consistent pattern appearing in many regions, except for northern Borneo (Fig. 5a, b) regions, is the predominant decreases in rainfall during inter-monsoon seasons, such as August–September–October (ASO, from boreal summer monsoon to boreal winter monsoon) and February–March–April (FMA, from boreal winter monsoon to boreal summer monsoon). This decreasing signal seems to be stronger in RCP8.5 than in RCP4.5 and is not a random feature appearing in a certain simulation driven by a specific GCM, but rather a robust pattern seen in all members driven by the three different GCMs. In addition, a majority of decreasing signal also satisfy the statistical significance at the 95% confidence level. This implies that the forced signal (e.g. rainfall decrease) in response to the RCP scenarios seems to overwhelm the internal variability (i.e., inter-annual and inter-decadal variability). On the other hand, the increasing rainfall feature appears intermittently, but its magnitude is not high and robustness in terms of statistical significance and model agreement is also very limited. More importantly, the change in rainfall along the annual cycle tends to be sensitive to latitudinal location of landmasses. While western part of Peninsula Malaysia and northern Sumatra exhibit a significant decrease in rainfall from February to April (e.g. boreal spring), southern Borneo, eastern part of Peninsula Malaysia, southern Sumatra and Java undergo much stronger decrease in rainfall from August and October (e.g. boreal fall). Interestingly, Singapore near the equator shows the decreasing rainfall signal in both boreal spring and fall seasons. Slight increase or no changes in rainfall during the wet season but significant decreases in rainfall during the inter-monsoon seasons result in the intensification of rainfall seasonality. Table 2 clearly shows this pattern of change in a quantitative manner. For the REF, eastern part of Peninsula Malaysia and Java show high seasonality due to a large difference between rainfall minima and maxima, implying a challenge in water reservoirs management. Furthermore, accelerated GHG concentration described by RCP8.5 emission scenario leads to more pronounced challenges of water stress in natural ecosystems, and water management in man-made systems. Except for Northern Sumatra, all other regions are projected to confront intensified seasonality of rainfall and the resultant water stress in warmer climates.

Table 2 Rainfall seasonality derived from historical, RCP4.5 and RCP8.5 over nine sub-region. Brackets indicate seasonality change (%)

Sub-region	TRMM	REF	RCP4.5	RCP8.5
A: Borneo (Northeast)	0.4	0.4	0.6 (50%)	0.6 (50%)
B: Borneo (Northwest)	0.9	0.9	0.9 (0%)	1.0 (11%)
C: Borneo (South)	0.7	0.6	0.7 (17%)	0.8 (33%)
D: Peninsula Malaysia (East)	1.4	1.1	1.5 (36%)	1.4 (27%)
E: Peninsula Malaysia (West)	0.8	0.8	1.0 (25%)	1.0 (25%)
F: Singapore	0.8	0.9	1.2 (33%)	1.2 (33%)
G: Sumatra (North)	0.7	0.6	0.6 (0%)	0.6 (0%)
H: Sumatra (South)	0.7	0.7	0.8 (14%)	1.1 (57%)
I: Java	1.5	1.5	1.5 (0%)	2.0 (33%)

To gain insight into the mechanism behind rainfall changes, we need to understand the asymmetric behavior within the annual cycle and along latitudinal locations. For further details of the characteristics of rainfall changes, we present the latitude-time cross section of zonally averaged (from 95°E to 119°E) total rainfall as well as convective and large-scale (non-convective) rainfall (Fig. 6). For the purpose of assessing the consistency among the MRCM_BC results driven by the three different GCMs, a perfect agreement between the three members in terms of the direction of the projected change are illustrated in stippling for each grid point.

Based on this analysis, the relative role of convective and large-scale rainfall in determining the changes in total rainfall can be identified. The most striking feature in both RCP4.5 and RCP8.5 is a remarkable decrease in total rainfall at the south of equator from August to October, which is attributed to the decreases in both convective and large-scale rainfall. In the case of RCP4.5, the increases in large-scale rainfall appear along the whole latitudinal band, but with no consistency among different three projections.

In the following, we focus on the detailed regional patterns and different behaviors of rainfall changes for wet season (NDJ) and inter-monsoon seasons (ASO and FMA). Figure 7 presents the spatial distribution of rainfall changes for wet season. The ensembles of projections from the GCMs and MRCM_BC are presented with the same format in order to compare the large-scale patterns between MRCM_BC projections and driving GCMs. Stippling marked for each grid point indicates the model agreement. It supports the

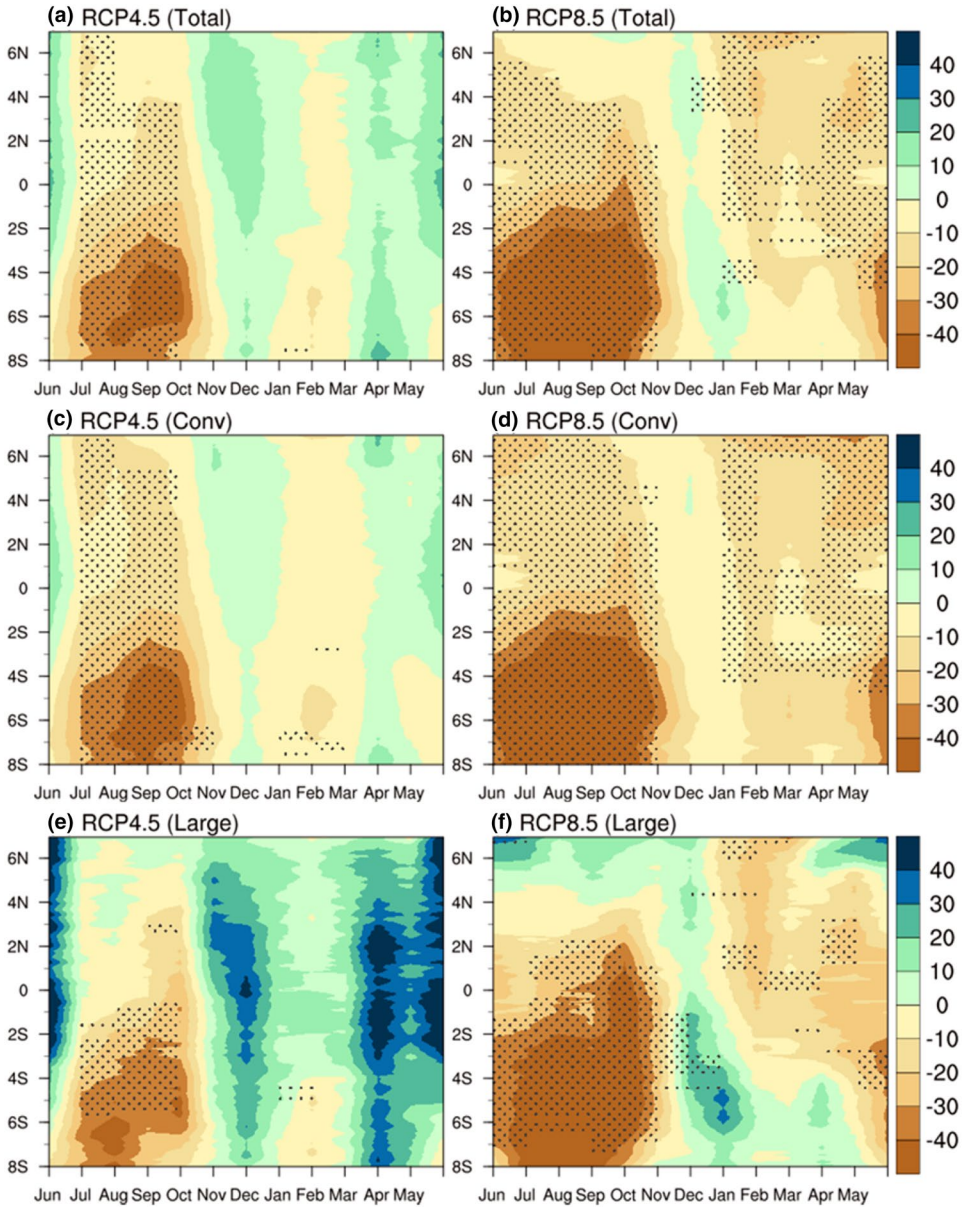

Fig. 6 Latitude-time cross section of monthly mean changes in total, convective, and large-scale rainfall averaged from 95°E to 119°E under (**a, c, e**) RCP4.5 and (**b, d, f**) RCP8.5. Stippled area indicates that three MRCMs agree in the sign of same signal (unit: %)

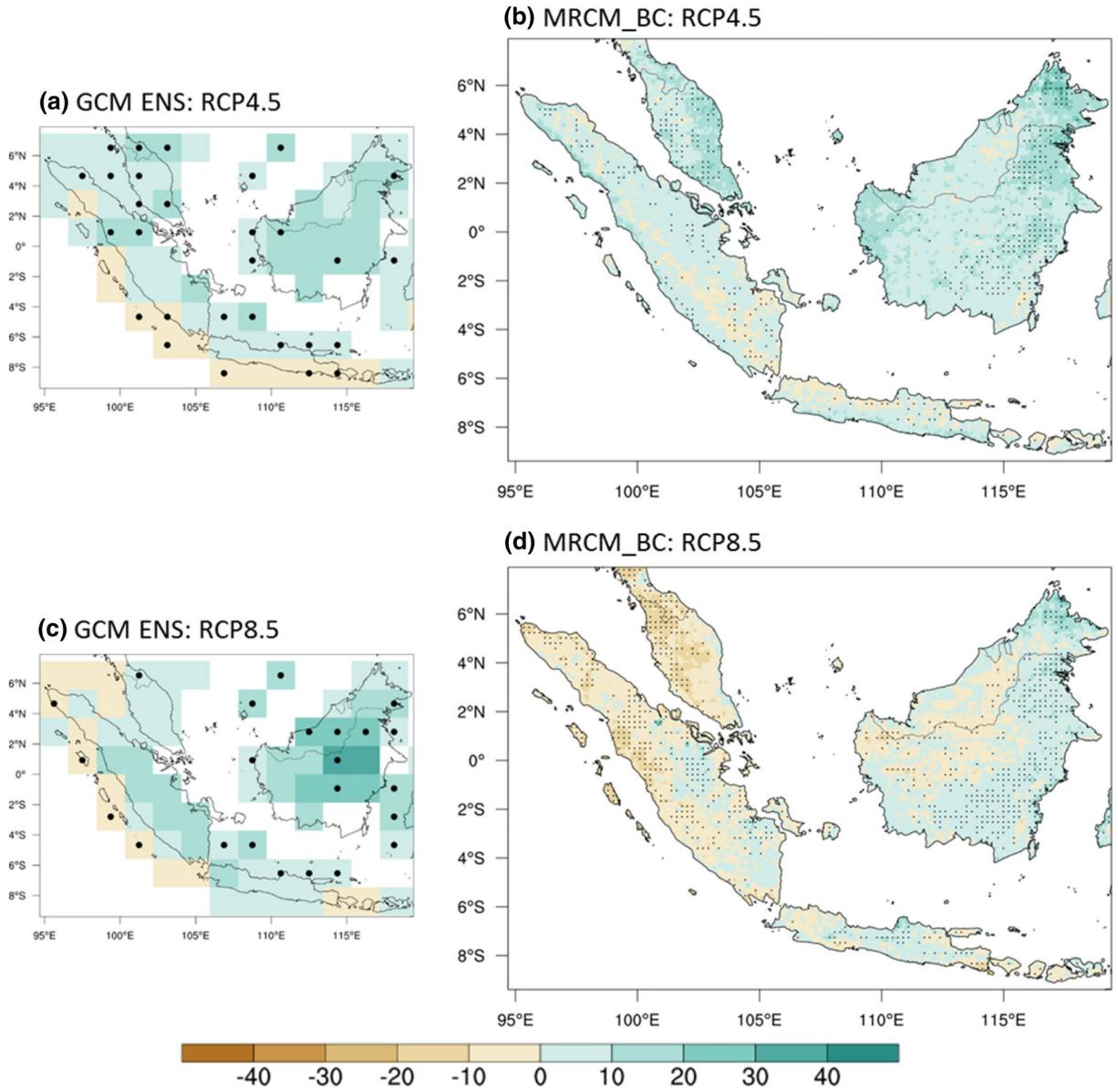

Fig. 7 NDJ mean percentage changes in ensemble mean rainfall for RCP4.5 and RCP8.5 from (**a, c**) GCMs (denoted by GCM ENS) and (**b, d**) MRCMs (denoted by MRCM_BC). Stippled area indicates that three GCMs (or MRCMs) agree in the sign of same signal (unit: %)

robustness of the conclusion that enhanced GHGs forcing can trigger a common response, with the same direction of change, in the three different GCMs. Consistent with the latitude-time cross section seen in Fig. 6, RCP4.5 projection shows that most regions are prone to increase in rainfall. Although there are some regions where three ensembles members all produce a consistent change signal of rainfall increase, other regions suffer from a lack of models agreement with relatively weak magnitudes of changes. For RCP8.5 projection, MRCM_BC shows quite mixed signals for the rainfall change.

Figures 8 and 9 present the spatial distribution of rainfall changes during inter-monsoon transitional seasons (ASO and FMA) and the dominance of rainfall decrease is clearly contrasted with rainfall changes for wet monsoon season. By comparing GCM projections between ASO and FMA, the increasing or decreasing sign of rainfall changes are flipped roughly along the equator, with very different magnitudes of the change. MRCM_BC shows a tendency to follow the GCM patterns, but exhibits more extended area with decrease in rainfall. MRCM seems to amplify the physical processes that lead to the favorable condition for rainfall inhibition under global warming (see the explanation in Figs. 10, 11). Although there is clear signal of rainfall decrease, the magnitude of change is significantly less in FMA than in ASO, supporting asymmetric

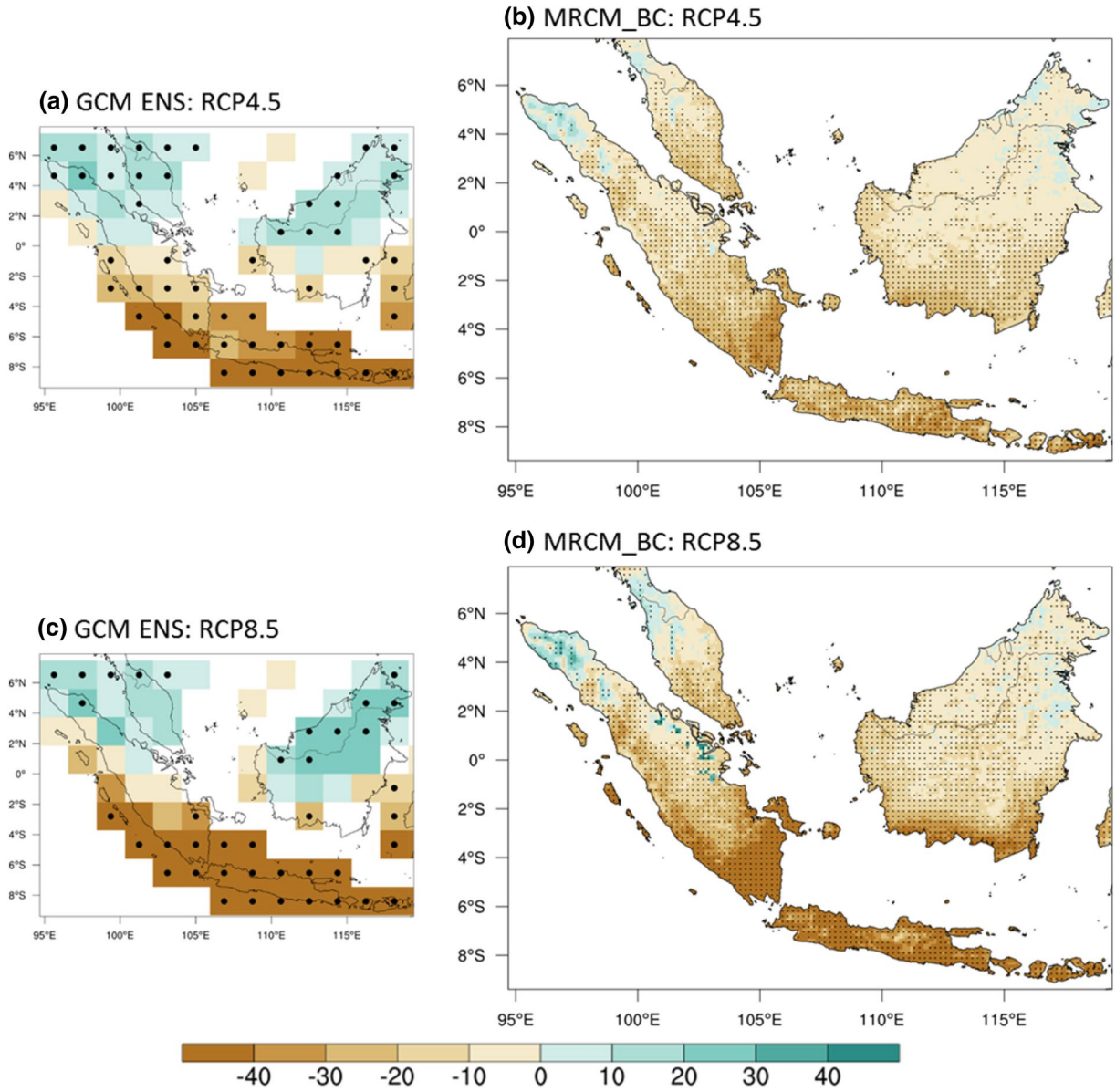

Fig. 8 ASO mean percentage changes in ensemble mean rainfall for RCP4.5 and RCP8.5 from (**a, c**) GCMs (denoted by GCM ENS) and (**b, d**) MRCMs (denoted by MRCM_BC). Stippled area indicates that three GCMs (or MRCMs) agree in the sign of same signal (unit: %)

pattern of rainfall changes within the annual cycle as seen in Figs. 5 and 6.

This reversed and asymmetric pattern can be partly explained by the dynamic components describing atmospheric vertical motion. Figures 10 and 11 present the omega (p velocity) for the REF and its future changes under RCP4.5 and RCP8.5 scenarios. For the REF of ASO, rising branches broadly occupied the whole northern part of the domain and sinking motion at the edge of southern boundary maintaining a meridional overturning circulation. As the seasons progress to FMA, the ascendance region and subsidence region are switched, leading to reversed circulation. An important point is that the strength of circulation in ASO is not held during FMA. Asymmetry of the seasonal march between boreal fall and boreal spring is attributed to the distribution of lower boundary between land and ocean and the differences between land and ocean in their thermal memories (Chang et al. 2005). The strength of circulation for REF is likely to determine the degree of future changes in response to rising concentration of GHGs. For RCP8.5 projection during ASO, the emergence of strong positive anomaly of omega is consistent with a large decrease of rainfall, particularly south of equator. By comparison, the change in omega is less relevant during FMA, again matching the rainfall change pattern. Back to the comparison of rainfall changes between MRCM_BC projections and driving GCM

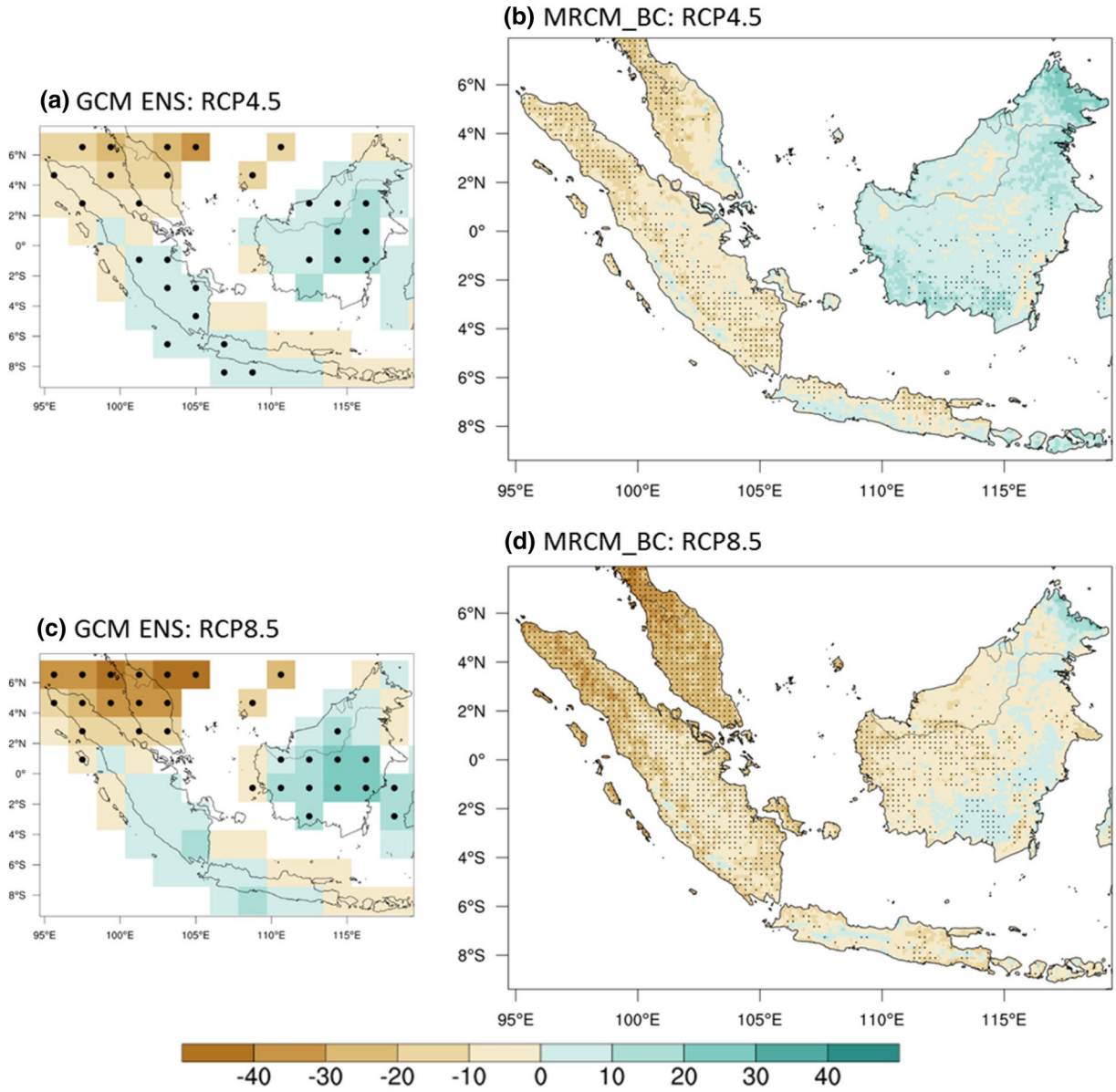

Fig. 9 FMA mean percentage changes in ensemble mean rainfall for RCP4.5 and RCP8.5 from (**a, c**) GCMs (denoted by GCM ENS) and (**b, d**) MRCMs (denoted by MRCM_BC). Stippled area indicates that three GCMs (or MRCMs) agree in the sign of same signal (unit: %)

projections, the decreases in rainfall are more significant in MRCM_BC than GCM. That is because the extent and magnitude of positive anomaly of omega is much less in the GCM (not shown) than in MRCM seen in Fig. 10c. A more realistic coastline and a sharp gradient of topography derived from higher resolution of MRCM are able to enhance the circulation and regional changes in response to the assumed forcing (e.g. rising concentration of GHGs) (Im and Eltahir 2017).

The different behavior in accordance with the low-level circulation between ASO and FMA seasons can be seen more clearly in Fig. 12 which presents the moisture flux and convergence at 850 hPa derived from REF and its change under RCP8.5 scenario. For REF, climatological moisture flux is apparently reversed between ASO and FMA, which in turn leads to the strong moisture convergence north and south of equator respectively. Under RCP8.5, anomalous flux is stronger in ASO than in FMA, which is in line with the magnitude of changes in rainfall and vertical motion. Most land area is dominated by low-level horizontal divergence, consistent with the vertical sinking motion.

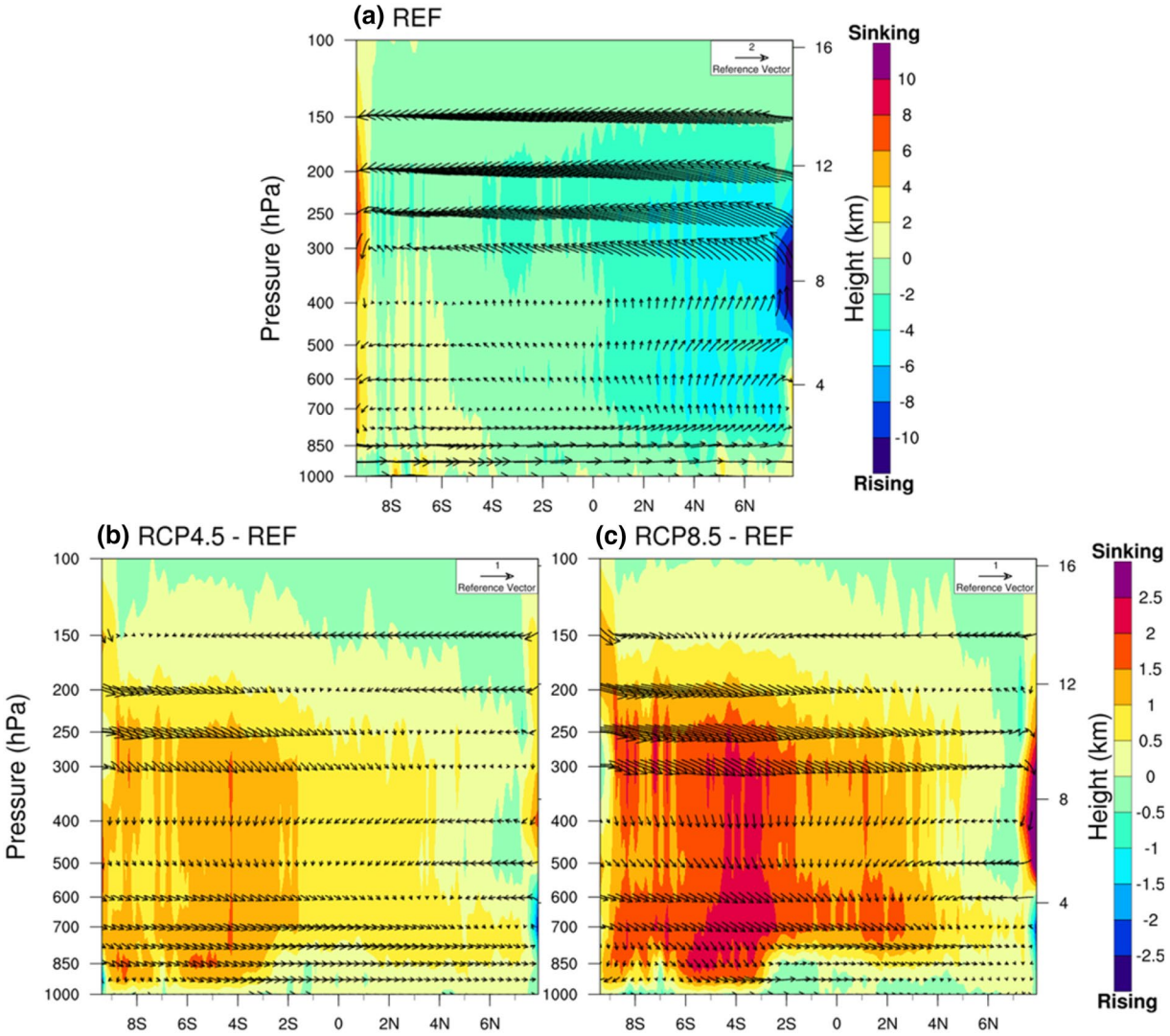

Fig. 10 Latitude-height cross sections of p velocity (omega, 10^{-3} Pa s^{-1}) and vector (v; w × 10^{-3}) zonally-averaged from 95°E to 119°E during ASO season derived from **a** REF and its change under **b** RCP4.5 and **c** RCP8.5

4 Summary and conclusions

In the study, the impact of climate change over the western Maritime Continent is investigated based on the regional climate projections dynamically downscaled using MRCM with 12 km horizontal resolution. The surface and lateral boundary conditions used to force MRCM are taken from three CMIP5 participant models, namely, CCSM4, MPI-ESM-MR, and ACCESS 1.0, which are selected through a screening process based on the model performance in simulating present-day climate, and its horizontal resolution. Dynamical downscaling using MRCM is conducted for a total of nine 31-year regional climate projections under multi-GCMs (CCSM4, MPI-ESM-MR, and ACCESS 1.0) and multi-scenarios of emission (REF: 1975–2005, RCP4.5, and RCP8.5: 2070–2100, first 1 year is used for spin-up). In order to enhance the reliability of future projections, the PQM method, which is widely used for statistical bias correction, is applied to MRCM raw data in order to minimize the systematic errors due to the imperfections of both MRCM physics and driving GCM forcings.

Based on validation analysis of ensemble mean of REF, the MRCM_BC provides added value over GCM and improved performance over MRCM both quantitatively and qualitatively. Seasonally averaged pattern and daily frequency distribution derived from the MRCM_BC reasonably agree with the TRMM observed rainfall patterns. Note that bias correction is not likely to significantly affect the future change pattern, in contrast with the significant difference in the performance of the REF. It is because the systematic bias of model can be mostly eliminated by subtracting the climatological mean of the REF from that of the RCP future

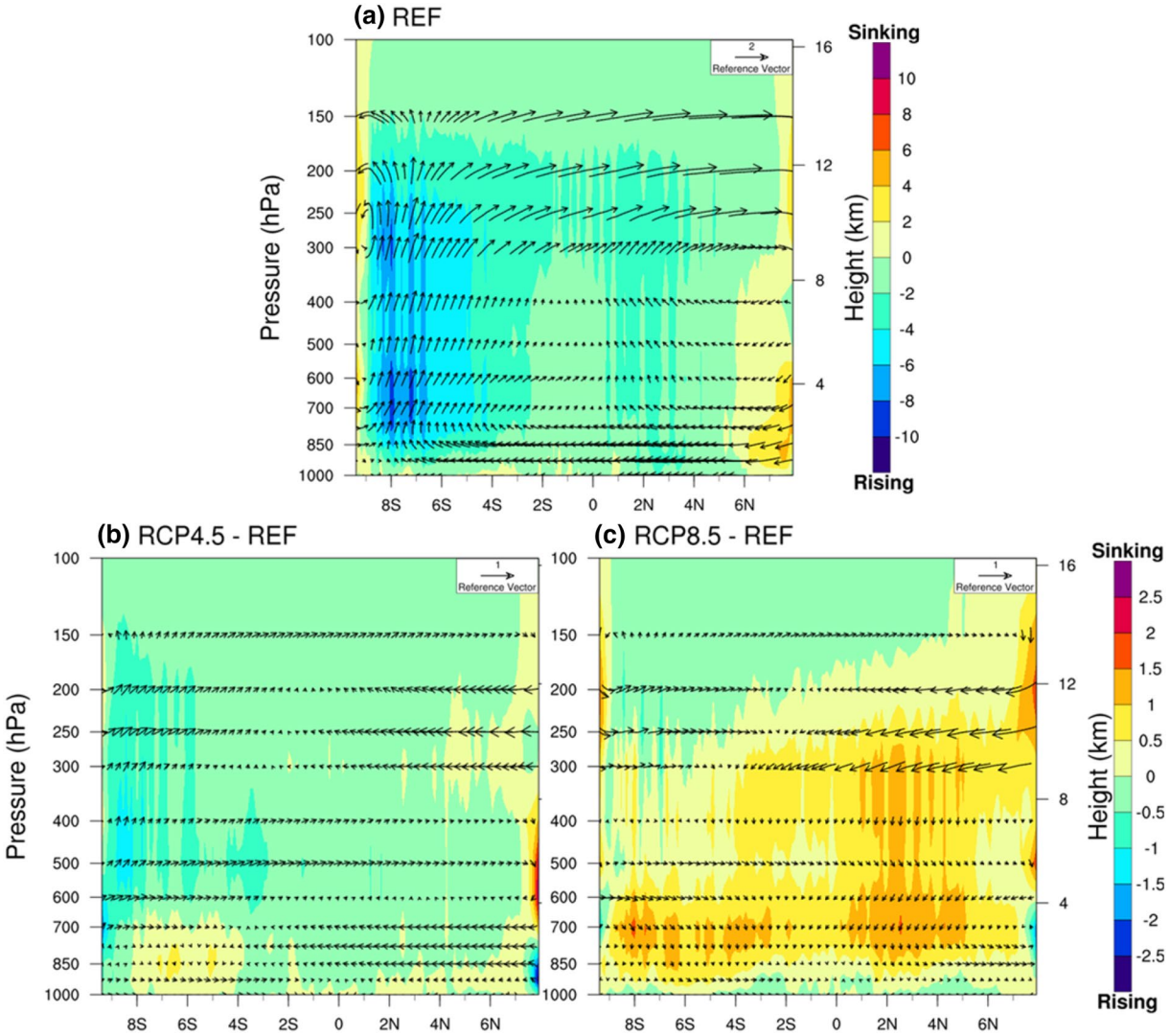

Fig. 11 Latitude-height cross sections of p velocity (omega, 10^{-3} Pa s^{-1}) and vector (v; w × 10^{-3}) zonally-averaged from 95°E to 119°E during FMA season derived from **a** REF and its change under **b** RCP4.5 and **c** RCP8.5

projections, under the assumption of "stationarity" that bias pattern does not change with time. Based on the projections used in this study, the future change patterns with and without bias correction are not much different in terms of climatological mean (not shown).

Under RCP4.5 and RCP8.5 scenarios, MRCM_BC projections show a significant decrease in rainfall with a high degree of robustness evident in the agreement among the three projections driven by different GCMs. More importantly, the pattern of projected change in the different seasons is characterized by asymmetric behavior varying between different latitudinal locations, north or south of equator. The decrease in rainfall is predominantly during the inter-monsoon seasons (e.g., ASO and FMA), however, the intensity and extent of change are different between ASO and FMA. A more significant decrease in rainfall is expected south of equator during ASO than north of equator during FMA. Interestingly, Singapore located near equator is likely to experience a decrease in rainfall in both ASO and FMA. The projected regional climate change features a more intense seasonality of rainfall, with potentially important implications for seasonal water stress of natural ecosystems, and new challenges for management of man-made reservoirs.

The main factor behind the projected rainfall changes can be at least partly explained by the changes in vertical atmospheric motion and associated meridional overturning circulation. Based on analysis of atmospheric vertical motion fields, the ascending motion of REF is weakened and or displaced by anomalous descending motion. The different strength of circulation between ASO and FMA for REF leads to different magnitudes of response under future

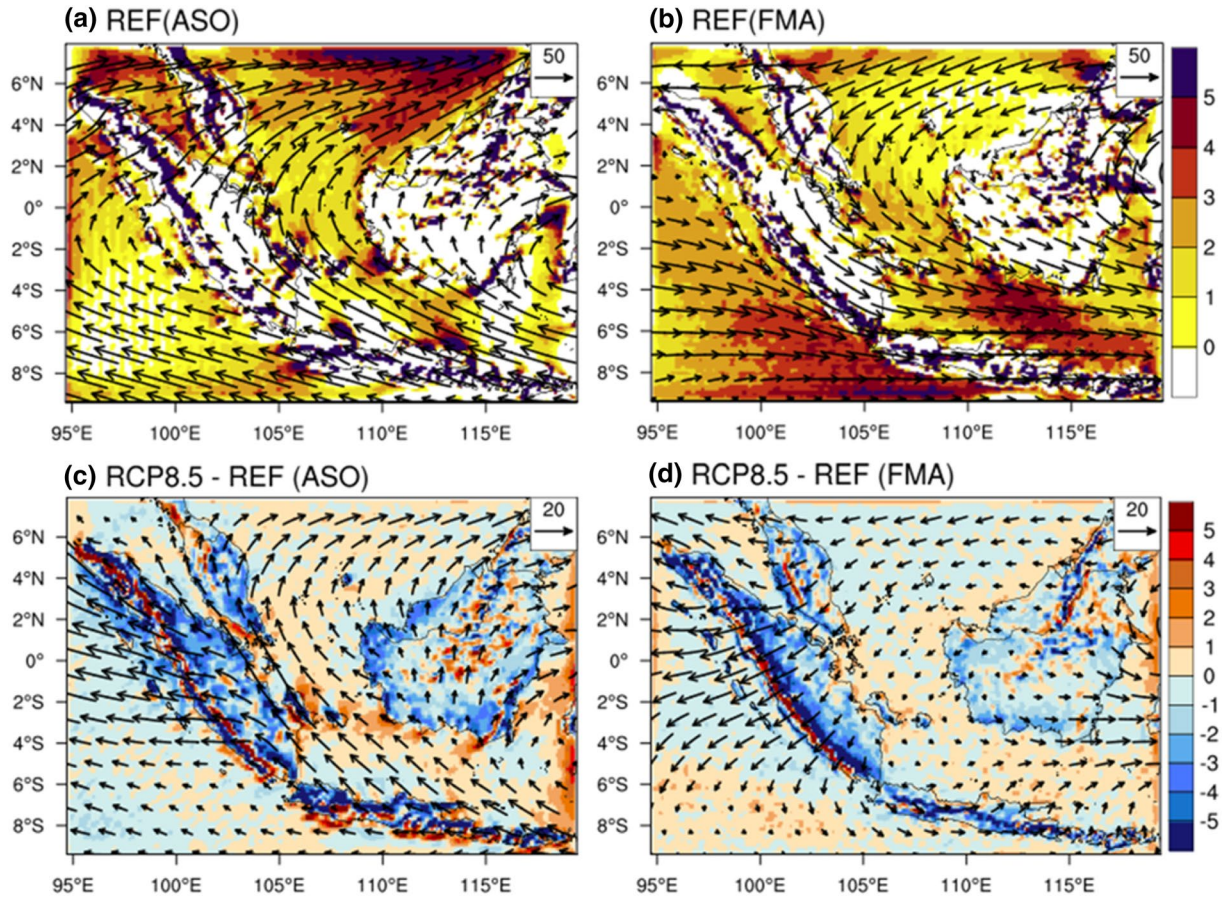

Fig. 12 Moisture flux (vector, g kg^{-1}m s^{-1}) with convergence and divergence (shading, 10^{-6} s^{-1}) at 850 hPa for reference period (REF) and its change under RCP 8.5 during (**a, c**) ASO and (**b, d**) FMA seasons

condition. RCP8.5 simulations project strong positive anomaly of omega, which is consistent with a large decrease of rainfall, particularly south of equator over the western Maritime Continent during ASO. Our conclusions are consistent with various studies on climate change (e.g., Vecchi and Soden 2007; Bony et al. 2013; Lau and Kim 2015) which suggested that rainfall is projected to decrease in tropical western Pacific due to ITCZ movement and weakening of Hadley circulation.

In this study, we attempt to provide a region-specific fine-scale climate projections that are produced to study climate change impacts over the western Maritime Continent. Projections of climate change under different scenarios are often dynamically downscaled using a high-resolution RCMs but mostly focusing on North America, Europe, and East Asia. In this regard, this research performed applying a state-of-the-art experimental framework (12 km resolution of RCM, multi-GCM driving forcings from CMIP5, multi-RCP scenarios) fills a gap in climate change research over this region, while effectively building on previous research by this group and other published studies.

Acknowledgements This research is supported by the National Research Foundation Singapore under its Campus for Research Excellence and Technological Enterprise programme. The Center for Environmental Sensing and Modeling is an interdisciplinary research group of the Singapore MIT Alliance for Research and Technology. The corresponding author, E.-S. Im, was supported by the Korea Agency for Infrastructure Technology Advancement (KAIA) Grant funded by the Ministry of Land, Infrastructure and Transport (Grant 18AWMP-B083066-05).

References

Aldrian E, Susanto RD (2003) Identification of three dominant rainfall regions within Indonesia and their relationship to sea surface temperature. Int J Climatol 23:1435–1452. https://doi.org/10.1002/joc.950

Arakawa O, Kitoh A (2005) Rainfall diurnal variation over the Indonesian Maritime Continent simulated by 20 km mesh GCM. SOLA 1:109–112. https://doi.org/10.2151/sola.2005-029

Ashok K, Guan Z, Yamagata T (2001) Impact of the Indian Ocean Dipole on the relationship between Indian Ocean monsoon rainfall and ENSO. Geophys Res Lett 28:4499–4502. https://doi.org/10.1029/2001GL013294

Bi D, Dix M, Marsl SJ, O'Farrell S, Rashid H, Uotila P, Hirst AC, Kowalczyk E, Golebiewski M, Sullivan A, Yan H, Hannah N, Franklin C, Sun Z, Vohralik P, Watterson I, Zhou X, Fiedler R, Collier M, Ma Y, Noonan J, Stevens L, Uhe P, Zhu H, Griffies SM, Hill R, Harris C, Puri K (2013) The ACCESS coupled model: description, control climate and evaluation. Aust Met Oceanog J 63:9–32

Bony S, Bellon G, Klocke D, Sherwood S, Fermepin S, Denvil S (2013) Robust direct effect of carbon dioxide on tropical circulation and regional precipitation. Nat Geosci 6:447–451. https://doi.org/10.1038/ngeo1799

Chang C-P, Wang Z, Ju J, Li T (2004) On the relationship between Western Maritime continent monsoon rainfall and ENSO during Northern Winter. J Clim 17:665–672. https://doi.org/10.1175/1520-0442(2004)017<0665:OTRBWM>2.0.CO;2

Chang C-P, Wang Z, McBride J, Liu CH (2005) Annual cycle of Southeast Asia-Maritime Continent rainfall and the asymmetric monsoon transition. J Clim 18:287–301. https://doi.org/10.1175/JCLI-3257.1

Chen T-C, Tsay J-D, Yen M-C, Matsumoto J (2013a) The winter rainfall of Malaysia. J Clim 26:936–958. https://doi.org/10.1175/JCLI-D-12-00174.1

Chen T-C, Tsay J-D, Yen M-C, Matsumoto J (2013b) Interannual variation of the winter rainfall in Malaysia. J Clim 26:4630–4648. https://doi.org/10.1175/JCLI-D-12-00367.1

Chotamonsak C, Salathé EP Jr, Kreasuwan J, Chantara S, Siriwitayakorn K (2011) Projected climate change over Southeast Asia simulated using a WRF regional climate model. Atmos Sci Let 12:213–219. https://doi.org/10.1002/asl.313

Christensen JH et al (2013) Climate phenomena and their relevance for future regional climate change. In: Stocker TF et al (eds) Climate change 2013: the physical science basis. Contribution of working group I to the fifth assessment report of the intergovernmental panel on climate change. Cambridge University Press, Cambridge, pp 1217–1308

Cruz FT, Narisma GT, Dado JM, Singhruck P, Tangang FT, Linarka UA, Wati T, Juneng L, Phan-Van T, Ngo-Duc T, Santisirisomboon J, Gunawan D, Aldrian E (2017) Sensitivity of temperature to physical parameterization schemes of RegCM4 over the CORDEX-Southeast Asia Region. Int J Climatol 37:5139–5153. https://doi.org/10.1002/joc.5151

Dee DP, Uppala SM, Simmons AJ, Berrisford P, Poli P, Kobayashi S, Andrae U, Balmaseda MA, Balsamo G, Bauer P, Bechtold P, Beljaars ACM, van de Berg L, Bidlot J, Bormann N, Delsol C, Dragani R, Fuentes M, Geer AJ, Haimberger L, Healy SB, Hersbach H, Hólm EV, Isaksen L, Kållberg P, Köhler M, Matricardi M, McNally AP, Monge-Sanz BM, Morcrette JJ, Park BK, Peubey C, de Rosnay P, Tavolato C, Thépaut JN, Vitart F (2011) The ERA-Interim reanalysis: configuration and performance of the data assimilation system. Q J R Meteorol Soc 137(656):553–597. https://doi.org/10.1002/qj.828

Ehret U, Zehe E, Wulfmeyer V, Warrach-Sagi K, Liebert J (2012) Should we apply bias correction to global and regional climate model data? Hydrol Earth Syst Sci Discuss 9:5355–5387. https://doi.org/10.5194/hessd-9-5355-2012

Gent PR et al (2011) The community climate system model version 4. J Clim 24(19):4973–4991. https://doi.org/10.1175/2011JCLI4083.1

Gianotti RL (2012) Convective cloud and rainfall processes over the Maritime Continent: simulation and analysis of the diurnal cycle. Ph.D. Dissertation, Massachusetts Institute of Technology, p 306

Gianotti RL, Eltahir EAB (2014a) Regional climate modeling over the Maritime Continent. Part I: new parameterization for convective cloud fraction. J Clim 27:1488–1503. https://doi.org/10.1175/JCLI-D-13-00127.1

Gianotti RL, Eltahir EAB (2014b) Regional climate modeling over the Maritime Continent. Part II: new parameterization for autoconversion of convective rainfall. J Clim 27:1504–1523. https://doi.org/10.1175/JCLI-D-13-00171.1

Giorgetta MA, Jungclaus J, Reick C, Legutke S, Bader J, Bttinger M, Brovkin V, Crueger T, Esch M, Fieg K, Glushak K, Gayler V, Haak H, Hollweg HD, Ilyina T, Kinne S, Kornblueh L, Matei D, Mauritsen T, Mikolajewicz U, Mueller W, Notz D, Pithan F, Raddatz T, Rast S, Redler R, Roeckner E, Schmidt H, Schnur R, Segschneider J, Six KD, Stockhause M, Timmreck C, Wegner J, Widmann H, Wieners KH, Claussen M, Marotzke J, Stevens B (2013) Climate and carbon cycle changes from 1850 to 2100 in MPI-ESM simulations for the coupled model intercomparison project phase 5. J Adv Model Earth Syst 5:572–597. https://doi.org/10.1002/jame.20038

Giorgi F, Coppola E, Solmon F, Mariotti L, Sylla MB, Bi X, Elguindi N, Diro GT, Nair V, Giuliani G, Cozzini S, Güttler I, O'Brien TA, Tawfik AB, Shalaby A, Zakey AS, Steiner AL, Stordal F, Sloan LC, Brankovic C (2012) RegCM4: model description and preliminary tests over multiple CORDEX domains. Clim Res 52:7–29. https://doi.org/10.3354/cr01018

Harris I, Jones P, Osborn T, Lister D (2014) Updated high-resolution grids of monthly climatic observations—the CRU TS3.10 dataset. Int J Climatol 34:623–642. https://doi.org/10.1002/joc.3711

Huffman GJ, Bolvin DT (2012) TRMM and other data precipitation data set documentation. Laboratory for Atmospheres, NASA Goddard Space Flight Center and Science Systems and Applications

Im E-S, Eltahir EAB (2017) Simulation of the diurnal variation of rainfall over the western Maritime Continent using a regional climate model. Clim Dyn. https://doi.org/10.1007/s00382-017-3907-3

Im E-S, Gianotti RL, Eltahir EAB (2014) Improving the simulation of the West African Monsoon using the MIT regional Climate Model. J Clim 27:2209–2229. https://doi.org/10.1175/JCLI-D-13-00188.1

Jamaluddin AF, Tangang F, Chung JX, Juneng L, Sasaki H, Takayabu I (2017) Investigating the mechanisms of diurnal rainfall variability over Peninsular Malaysia using the non-hydrostatic regional climate model. Meteorol Atmos Phys. https://doi.org/10.1007/s00703-017-0541-x

Juneng L, Tangang FT (2005) Evolution of ENSO-related rainfall anomalies in Southeast Asia region and its relationship with atmosphere-ocean variations in Indo-Pacific sector. Clim Dyn 25:337–350. https://doi.org/10.1007/s00382-005-0031-6

Juneng L, Tangang FT (2010) Long-term trends of winter monsoon synoptic circulations over the maritime continent: 1962–2007. Atmos Sci Lett 11:199–203. https://doi.org/10.1002/asl.272

Juneng L, Tangang F, Chung J et al (2016) Sensitivity of Southeast Asia rainfall simulations to cumulus and air-sea flux parameterizations in RegCM4. Clim Res 69:59–77. https://doi.org/10.3354/cr01386

Lau WKM, Kim KM (2015) Robust Hadley circulation changes and increasing global dryness due to CO_2 warming from CMIP5 model projections. Proc Natl Acad Sci USA 112:3630–3635. https://doi.org/10.1073/pnas.1418682112

Liang XZ, Li L, Dai A, Kunkel KE (2004) Regional climate model simulation of summer precipitation diurnal cycle over the United States. Geophys Res Lett 31:L24208. https://doi.org/10.1029/2004GL021054

Liang XZ, Kunkel KE, Meehl GA, Jones RG, Wang JXL (2008) Regional climate models downscaling analysis of general circulation models present climate biases propagation into future change projections. Geophys Res Lett 35:L08709. https://doi.org/10.1029/2007GL032849

Loh JL, Tangang F, Juneng L, Hein D, Lee D-I (2016) Projected rainfall and temperature changes over Malaysia at the end of the 21st century based on PRECIS modelling system. Asia Pac J Atmos Sci 52:191–208. https://doi.org/10.1007/s13143-016-0019-7

Love BS, Matthews AJ, Lister GMS (2011) The diurnal cycle of precipitation over the Maritime Continent in a high-resolution atmospheric model. Q J R Meteorol Soc 137:934–947. https://doi.org/10.1002/qj.809

Lucas-Picher P, Somot S, Déqué M, Decharme B, Alias A (2013) Evaluation of the regional climate model ALADIN to simulate the climate over North America in the CORDEX framework. Clim Dyn 41:1117–1137. https://doi.org/10.1007/s00382-012-1613-8

Marcella M, Eltahir EAB (2012) Modeling the summertime climate of Southwest Asia: the role of land surface processes in shaping the climate of semiarid regions. J Clim 25:704–719. https://doi.org/10.1175/2011JCLI4080.1

Marcella M, Eltahir EAB (2014) Introducing an irrigation scheme to a regional climate model: a case study over West Africa. J Clim 27:5708–5723. https://doi.org/10.1175/JCLI-D-13-00116.1

Mariotti L, Diallo I, Coppola E, Giorgi F (2014) Seasonal and intraseasonal changes of African monsoon climates in 21st century CORDEX projections. Clim Change 125:53–65. https://doi.org/10.1007/s10584-014-1097-0

McSweeney CF, Jones RG, Lee RW, Rowell DP (2015a) Selecting CMIP5 GCMs for downscaling over multiple regions. Clim Dyn 44:3237–3260. https://doi.org/10.1007/s00382-014-2418-8

McSweeney CF et al (2015b) Singapore's second national climate change study—climate projections to 2100 science report. Centre for Climate Research Singapore, Chap. 4

Moron V, Robertson AW, Boer R (2009) Spatial coherence and seasonal predictability of monsoon onset over Indonesia. J Clim 22:840–850. https://doi.org/10.1175/2008JCLI2435.1

Moss RH, Edmonds JA, Hibbard KA, Manning MR, Rose SK, van Vuuren DP, Carter TR, Emori S, Kainuma M, Kram T, Meehl GA, Mitchell JFB, Nakicenovic N, Riahi K, Smith SJ, Stouffer RJ, Thomson AM, Weyant JP, Wilbanks TJ (2010) The next generation of scenarios for climate change research and assessment. Nature 463(7282):747–756. https://doi.org/10.1038/nature08823

Neale RB, Slingo JM (2003) The Maritime Continent and its role in the global climate: a GCM study. J Clim 16:834–848. https://doi.org/10.1175/1520-0442(2003)016<0834:TMCAIR>2.0.CO;2

Pal JS, Giorgi F, Bi X, Elguindi N, Solmon F, Gao X, Rauscher S, Francisco R, Zakey A, Winter J, Ashfaq M, Syed FS, Bell JL, Diffenbaugh NS, Karmacharya J, Konaré A, Martinez D, da Rocha RP, Sloan LC, Steiner AL (2007) The ICTP RegCM3 and RegCNET: regional climate modeling for the developing world. BAMS 88:1395–1409. https://doi.org/10.1175/BAMS-88-9-1395

Park C, Min S-K, Lee D et al (2016) Evaluation of multiple Regional Climate Models for summer climate extremes over East Asia. Clim Dyn 46:2469–2486. https://doi.org/10.1007/s00382-015-2713-z

Peatman SC, Matthews AJ, Stevens DP (2015) Propagation of the Madden–Julian oscillation and scale interaction with the diurnal cycle in a high-resolution GCM. Clim Dyn 45:2901–2918. https://doi.org/10.1007/s00382-015-2513-5

Piani C, Haerter JO, Coppola E (2010) Statistical bias correction for daily precipitation in regional climate models over Europe. Theor Appl Climatol 99:187–192. https://doi.org/10.1007/s00704-009-0134-9

Ploshay J, Lau N-C (2010) Simulation of the diurnal cycle in tropical rainfall and circulation during boreal summer with a high-resolution GCM. Mon Weather Rew 138:3434–3452. https://doi.org/10.1175/2010MWR3291.1

Qian JH (2008) Why precipitation is mostly concentrated over islands in the maritime continent. J Atmos Sci 65:1428–1441. https://doi.org/10.1175/2007JAS2422.1

Robertson AW, Moron V, Qian J-H, Chang C-P, Tangang F, Aldrian E, Koh TY, Juneng L (2011) The maritime continent monsoon. In: Chang CP et al (eds) The global monsoon system: research and forecast, 2nd edn. World Scientific Publishing Co., New Jersey, pp 85–98

Salimun E, Tangang F, Juneng L, Behera SK, Yu W (2014) Differential impacts of conventional El Niño versus El Niño Modoki on Malaysian rainfall anomaly during winter monsoon. Int J Climatol 34:2763–2774. https://doi.org/10.1002/joc.3873

Salimun E, Tangang F, Juneng L, Zwiersb FW, Merryfield WJ (2015) Skill evaluation of the CanCM4 and its MOS for seasonal rainfall forecast in Malaysia during the early and late winter monsoon periods. Int J Climatol 36:439–454. https://doi.org/10.1002/joc.4361

Schiemann R, Demory ME, Mizielinski MS, Roberts MJ, Shaffrey LC, Strachan J, Vidale PL (2014) The sensitivity of the tropical circulation and Maritime Continent precipitation to climate model resolution. Clim Dyn 42:2455–2468. https://doi.org/10.1007/s00382-013-1997-0

Smith A, Lott N, Vose R (2011) The integrated surface database: recent developments and partnerships. Bull Am Meteorol Soc 92:704–708. https://doi.org/10.1175/2011BAMS3015.1

Solman SA, Nu´n˜ ez MN, Cabre´ MF (2008) Regional climate change experiments over southern South America. I: present climate. Clim Dyn 30:533–552. https://doi.org/10.1007/s00382-007-0304-3

Tangang FT, Juneng L, Salimun E et al (2008) On the roles of the northeast cold surge, the Borneo Vortex, the Madden-Julian Oscillation, and the Indian Ocean Dipole during the extreme 2006/2007 flood in southern Peninsular Malaysia. Geophys Res Lett 35:L14S07. https://doi.org/10.1029/2008GL033429

Tangang FT, Juneng L, Salimun S, Kwan MS, Loh JL, Muhamad H (2012) Climate change and variability over Malaysia: gaps in science and research information. Sains Malays 41:1355–1366

Tangang FT, Farzanmanesh R, Mirzaei A, Supari, Salimun E, Jamaluddin AF, Juneng L (2017) Characteristics of precipitation extremes in Malaysia associated with El Niño and La Niña events. Int J Climatol 37:696–716. https://doi.org/10.1002/joc.5032

Taylor KE, Stouffer RJ, Meehl GA (2012) An overview of CMIP5 and the experiment design. Bull Am Meteorol Soc 93:485–498. https://doi.org/10.1175/BAMS-D-11-00094.1

Teo C-K, Koh T-Y, Lo JC-F, Bhatt BH (2011) Principal component analysis of observed and modeled diurnal rainfall in the Maritime Continent. J Clim 24:4662–4675

Vautard R, Gobiet A, Jacob D, Belda M, Colette A, Déqué M, Fernández J, García-Díez M, Goergen K, Güttler I et al (2013) The simulation of European heat waves from an ensemble of regional climate models within the EURO-CORDEX project. Clim Dyn 41:1–21. https://doi.org/10.1007/s00382-013-1714-z

Vecchi GA, Soden BJ (2007) Global warming and the weakening of the tropical circulation. J Clim 20:4316–4340. https://doi.org/10.1175/JCLI4258.1

Wang B, Wu R, Li T (2003) Atmosphere-warm ocean interaction and its impacts on Asian–Australian monsoon variation. J Clim 16:1195–1211. https://doi.org/10.1175/1520-0442(2003)16<1195:AOIAI>2.0.CO;2

Winter JM, Pal JS, Eltahir EAB (2009) Coupling of integrated biosphere simulator to regional climate model version 3. J Clim 22:2743–2756. https://doi.org/10.1175/2008JCLI2541.1

Zhou L, Wang Y (2006) Tropical Rainfall Measuring Mission observation and regional model study of precipitation diurnal cycle in the New Guinean region. J Geophys Res 111:D17104. https://doi.org/10.1029/2006JD007243